

¹ Mothana
Razzaq
Ibrahim

² Isam
Mahmood
Abdulbaqi

A Comparative Study of Different Induction Coils Used for Brazing Purposes



Abstract: - Brazing of copper tubes or copper pieces is widely used in industry for different applications. This study deals with a design of different complicated and non-traditional shapes and geometries of induction coils such that they will match the same power supply. Two shapes of induction coils (Coil A and Coil B) were designed and simulated. The design of each coil is done using the Electromagnetic–Thermal coupled algorithm adopting the finite element method (FEM) through ANSYS computer package. The real coils are tested practically to determine their inductance and resonance frequency. Different voltages and frequencies applied to each coil in order to obtain the best operating point. The results are documented and discussed, the practical results are well matched with the theoretical one. The results show that Coil B is more effective than Coil A, consume less power and complete the job in less time.

Keywords: Induction Brazing, Coil design, ANSYS, FEM.

I. INTRODUCTION

The induction heating (IH) technology is commonly used in industrial applications. This is done by applying an alternating voltage of certain frequency across an induction coil (IC) to produce an alternating magnetic flux affecting the specimen considered as a core in that IC. This will induce alternating eddy currents in the specimen at the same frequency as that of the IC voltage. Faraday's and Lenz's laws are the basis of induction heating [1], [2]. The Joule effect will generate heat due to the induced eddy currents. The design process of IC must handle a number of issues, including simulation of the required coil and its thermal operation during the heating process [3], [4].

The goal of this research is to design and simulate two shapes of IC mounted to a handheld welding instrument used for brazing copper tubes and copper pieces by IH. This instrument can be powered by a standard single phase, 220 V, 50 Hz power supply or by a battery or a solar photovoltaic (PV) panel [5]. This device is intended for usage in remote places when traditional electric power is unavailable. Despite its acceptable efficiency, this handheld welding instrument has a simple design, light weight, low price, and flexible.

A Self tuned single-phase inverter is used as a high frequency power source to feed power for the parallel tank circuit composed of the IC and a suitable parallel capacitor is able to determine the equivalent circuit of the IC practically [6]. To select the appropriate inverter, as a power supply for this handheld welding instrument, the following information must be available about the load (the tank circuit):

1. The required current for the brazing process at the predetermined time.
2. The required frequency.

The step preceding the design of the power supply is the simulation of the brazing process including the electromagnetic-thermal coupled analysis. This step will afford the required data mentioned above, because the tank circuit is the only load of this power supply, and its operation throughout the brazing process must be examined as a prior step [7].

To design an IC for this purpose, the flux distribution and eddy currents created in the copper tube components under process must be determined using Maxwell's equations, which are partial differential equations [8]. A transient thermal study must be performed after this stage to evaluate the heat spreading caused by these eddy currents. Then the electromagnetic-thermal coupled of the brazing procedure must be performed. To do so, the Finite Element Method (FEM) was used to numerically solve the relevant equations. The computer package ANSYS R17.0 was used to complete the FEM solution [9], [10], [11].

The literature on this issue is only some. In [12], khazaal designed and simulated an IC of cylindrical shape 13 turn, this furnace used for brazing two copper solid rods. In [13], Dragomir and Nikolay, design a butterfly coil and examines the computer forming of complex inductors using Comsol Multiphysics. In [14], Hanan designed a single turn coil and simulated by ANSYS. In [15], Aziz designed a spoon shape open sided coil and simulated by ANSYS.

II. THEORETICAL BACKGROUND

A. Electromagnetic Analysis

Maxwell equations that explain this phenomenon include:

¹ Electrical Engineering Department, Mustansiriya University, Baghdad-Iraq. eema2008@uomustansiriya.edu.iq

² Electrical Engineering Department, Mustansiriya University, Baghdad-Iraq. embaki56@uomustansiriya.edu.iq
Copyright © JES 2024 on-line : journal.esrgroups.org

Ampere's circuital law [8]:

$$\nabla \times \vec{H} = \vec{J} + \frac{\partial \vec{D}}{\partial t} \quad (1)$$

Faraday's law of induction:

$$\nabla \times \vec{E} = -\frac{\partial \vec{B}}{\partial t} \quad (2)$$

Gauss's law for magnetism:

$$\nabla \cdot \vec{B} = 0 \quad (3)$$

Gauss's law:

$$\nabla \cdot \vec{D} = \rho \quad (4)$$

\vec{H} = The magnetic field intensity, in $A \cdot m^{-1}$.

\vec{J} = The current density inside the specimen, in $A \cdot m^{-2}$.

\vec{D} = The electric flux density, in $C \cdot m^{-2}$.

\vec{E} = The electric field intensity, in $V \cdot m^{-1}$.

\vec{B} = The magnetic flux density, in $Wb \cdot m^{-2}$.

ρ = The electric charge density, in $C \cdot m^{-3}$.

Also,

$$J = \sigma E \quad (5)$$

$$D = \epsilon_0 \epsilon_r E \quad (6)$$

$$B = \mu_0 \mu_r H \quad (7)$$

ϵ_0 = The permittivity of vacuum, in $F \cdot m^{-1}$.

ϵ_r = The relative permittivity of material.

μ_0 = The permeability of vacuum, in $H \cdot m^{-1}$.

μ_r = The relative permeability of material.

σ = The material's conductivity when it is being heated (the workpiece), in $S \cdot m^{-1}$.

Since J is larger than the displacement current and the induction heating frequencies are often less than 10 MHz, it is necessary to ignore the right term $\left(\frac{\partial \vec{D}}{\partial t}\right)$ in equation (1)[18]. In addition, the specimen's power per unit volume may be represented as follows by ignoring the hysteresis losses in a copper specimen and using other mathematical manoeuvres:

$$Q_{induction} = \frac{|J_{eddy}|^2}{\sigma_{core}} \quad (8)$$

$Q_{induction}$ = The amount of power generated by the induced eddy currents in the workpiece per unit volume, in $W \cdot m^{-3}$.

B. Thermal Analysis

The thermal transient analysis uses the results of the electromagnetic steady-state analysis to determine the temperature distribution within the specimen using the Fourier equation below:

$$\rho_m C_p \frac{\partial T}{\partial t} = k \nabla^2 T + Q_{induction} \quad (9)$$

ρ_m = The specimen metal density, in $kg \cdot m^{-3}$.

C_p = The specific heat of the specimen, in $kJ \cdot kg^{-1} \cdot ^\circ C^{-1}$.

T = The temperature, in $^\circ C$.

k = The thermal conductivity of the workpiece metal, in $W \cdot m^{-1} \cdot ^\circ C^{-1}$.

The temperature inside the workpiece and on its surface is uniform and equal to the ambient temperature in its starting state at time ($t = 0$). However, due to the workpiece shape, its radiation ability to the space, and the turbulence of the air around it, the distribution changes during the heating process [16]. These circumstances change the equation (9) solution. The following formula results from including these components' effects in the equation:

$$\rho_m C_p \frac{\partial T}{\partial t} = k \nabla^2 T + Q_{induction} - \xi \sigma_s (T^4 - T_{air}^4) - \alpha (T - T_{air}) \tag{10}$$

ξ = The surface emissivity of the workpiece.

σ_s = Stefan-Boltzman constant.

α = The transfer coefficient of the workpiece, in $W \cdot m^{-2} \cdot K^{-1}$.

T_{air} = The temperature of the air, in °C.

C. Eddy Current and Skin Effect

When eddy currents are generated inside the workpiece by applying an alternating current, the induction heating process is carried out [17], [20]. Eddy current can be distributed asymmetrically, which is known by skin effect. The current density in this phenomena is hardly detectable in the middle and almost close to the workpiece's surface [2], [4].

III. DESIGN IMPLEMENTATION

A 3D FE analysis as a numerical method is applied using the ANSYS computer package as a solver of partial differential equations is well recognized [18]. By solving Maxwell and heat transfer equations, this method is considered to simulate the electromagnetic-thermal coupled analysis of the brazing process [22]. Only a computer program that follows the flowchart presented in Figure 1 can achieve this goal [19].

The load is a tank circuit made up of an induction coil and its (workpiece), which are the copper tube portions to be joined, connected in parallel to the tank capacitor. The brazing coil surrounds the the welding position coated by a thin strip of a Brazing Filler Metal (BFM) type (BAg-1) as a brazing catalyst [7]. This catalyst must be heated to its melting temperature of 618 °C to perform the brazing. To examine how the induced eddy currents are distributed inside the workpiece, the 3-D FE model must perform a steady-state electromagnetic analysis [12], [16], [21].

The following parameters must be determined when designing such coils:

1. The size of the copper tube used to wound the IC.
2. The required current passing through it.
3. The necessary frequency for such a brazing procedure.
4. The period of time it takes to complete the brazing procedure.
5. The induction coil's equivalent circuit parameters ($R-L$).

These parameters can be established by creating a 3-D finite element (FE) model for the copper tube to be welded, and the brazing process is performed using an induction coil [23], [24]. The magnetic field distribution and eddy currents induced in the copper tube portions to be joined are calculated using Maxwell's equations. According to the flow chart provided in Figure 1 that explains this iterative process, these data are transferred to the related thermal analysis to compute the heat distribution in the workpiece to be joined.

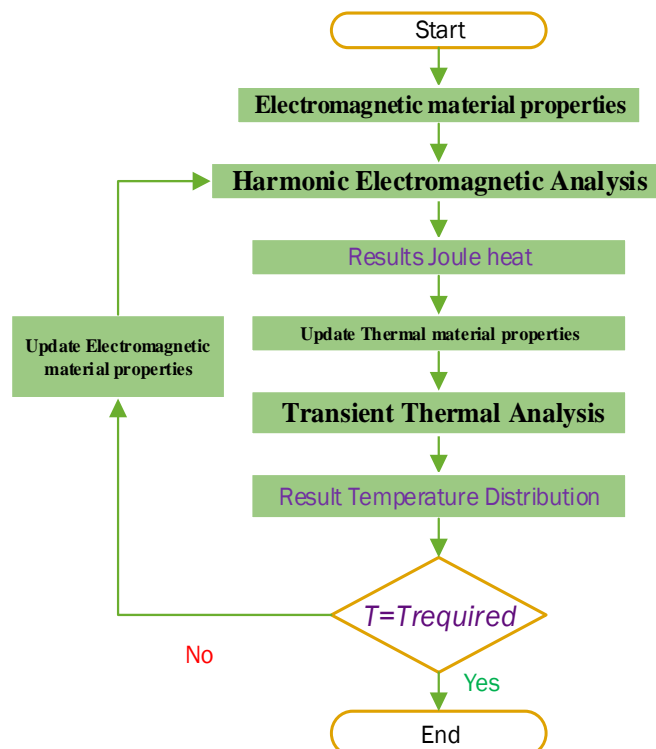


Fig. 1 The electromagnetic-thermal coupled analysis flow chart.

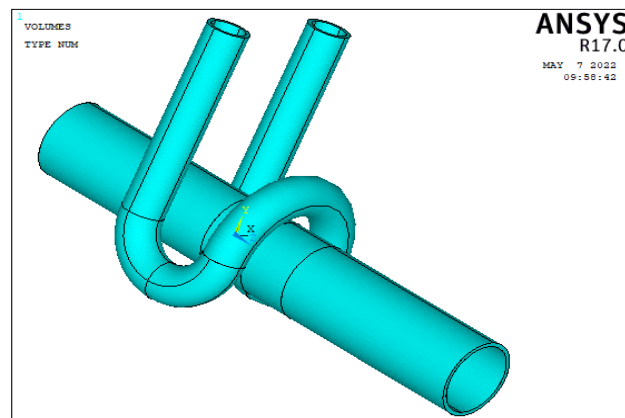
Two coils are designed with different shapes, simulated to show their different performances, using the same copper pipe cross section, air gap applied, and the same workpiece. The simulation reveals that the current and frequency for coil A to perform the process in (57) seconds are 1324 A and 34 kHz respectively, while those for Coil B are 328 A, 18.5 kHz, and (56) seconds. When Coil B is tested practically in lab. It reaches the melting point of the catalyst 618 °C in 52 s, 328 A, 141.42 V.

A. The Workpiece

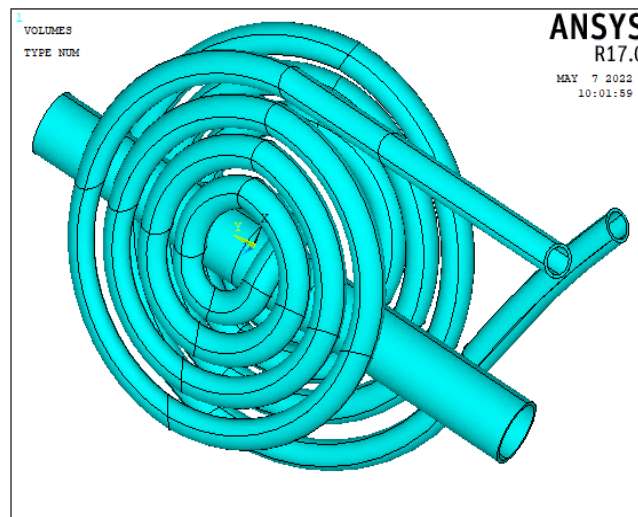
The most popular pipe used in industrial factories and any other kind of buildings were chosen to be the workpiece, which is a two pieces of copper tube required to be brazed, with outer diameter of 8 mm and inner diameter of 7 mm. as shown in Figure 2(a) and (b).

B. Coil A

The shape of Coil A as shown in Figure 2(a) is open sided, butterfly, single turn, hollow pipe, the outer diameter is 4 mm and the inner diameter is 3 mm. The mesh of Coil A with the workpiece is shown in Figure 3(a).



(a)

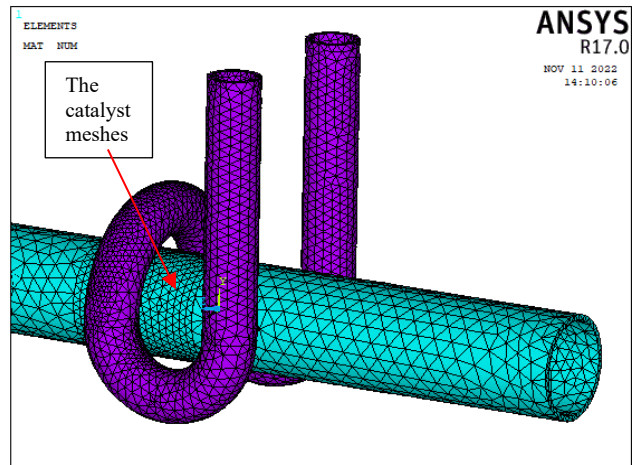


(b)

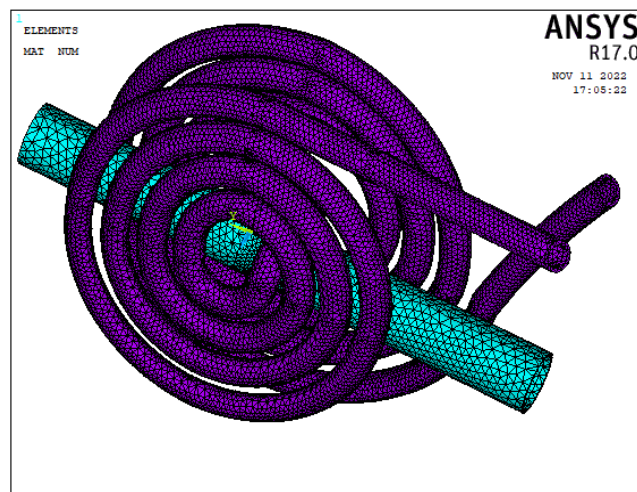
Fig. 2 The shape of coil A and B with the workpiece (a) Coil A (b) Coil B

C. Coil B

The shape of Coil B as shown in Figure 2(b) is open sided, butterfly, with two sides, each side is of multi-turn and of spiral shape, hollow pipe, the outer diameter is 4 mm and the inner diameter is 3 mm. The mesh of Coil B with the workpiece is shown in Figure 3(b).



(a)



(b)

Fig. 3 The mesh of induction coil and the workpiece (a) Coil A (b) Coil B

IV. DETERMINATION OF THE COILS BEST OPERATING CONDITION

Table 1 shows the simulation results of both coils by selecting the tank voltage equal to $V_{tank_{max}} = 260$ V, and tested at five different resonance frequencies. The results of Coil A show that, the first value at 10 kHz and 20 kHz are not accepted in spite of short brazing time due to the limitation of the coil current ($I_{c_{rms}}$). Also, the fifth value is not accepted due to the long brazing time. Coil B show an acceptable result at 20 kHz.

To use Coil A, it is recommended to raise the applied voltage across it and raising the operating frequency too in order to achieve an acceptable brazing time. The results for $V_{tank_{max}} = 400$ V and $f = 34$ kHz for coil A show a 56 second to heat the catalyst (BAg-1) to its melting point of 618 °C as shown in Figure 4 (a), while Coil B at tank voltage of $V_{tank_{max}} = 200$ V with frequency 18.5 kHz reaches the same temperature at 56 seconds as shown in Figure 4(b).

TABLE I
A Comparison Between Coils A and B Fed by 200 V_{max} at Different Frequencies

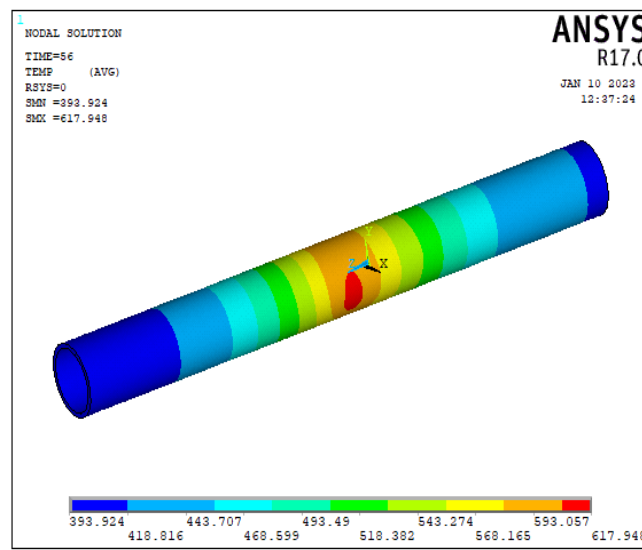
Coil A (open side one turn), $L=1 \mu\text{H}$			
f (kHz)	X_L (Ω)	$I_{c_{max}}$ (A)	time (s)
10	0.063	4127	18
20	0.126	2063	68
30	0.188	1382	130
40	0.251	1035	197
50	0.314	828	260
Coil B (two sides spiral), $L=3.7 \mu\text{H}$			

f (kHz)	X_L (Ω)	I_{cmax} (A)	time (s)
10	0.232	1120	13
20	0.465	559	33
30	0.697	373	55
40	0.93	279	76
50	1.162	223	98

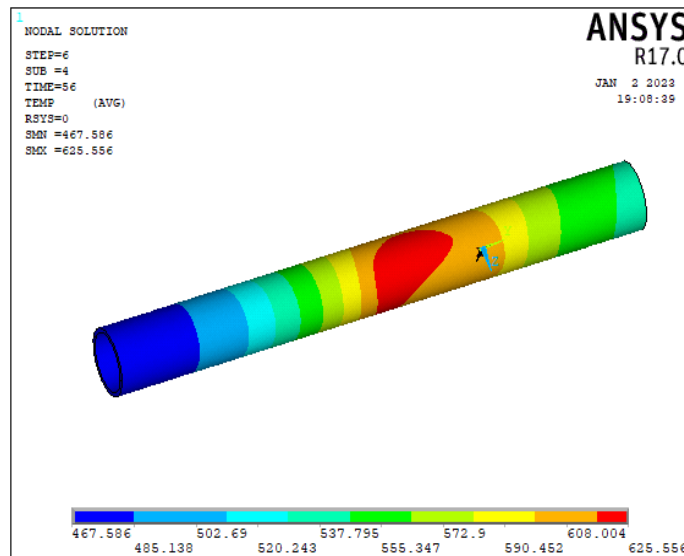
There is a difference in the temperature between the middle point of copper pipe (the BAg-1 position) and the end of the pipe shown in about 180 °C in both cases as shown in Figure 5.

V. PRACTICAL CONSIDERATIONS

The practical implementation of the designed coils according to the obtained simulation results must consider the impact of the real fabrication of the IC and the connection requirements with the parallel tank capacitor as shown in Figure 6 (a) and (b). The practical consideration of the manufactured coil and the real connected parts to the required tank capacitor affecting the value of the series resistance with the IC inductance in the equivalent circuit.



(a)

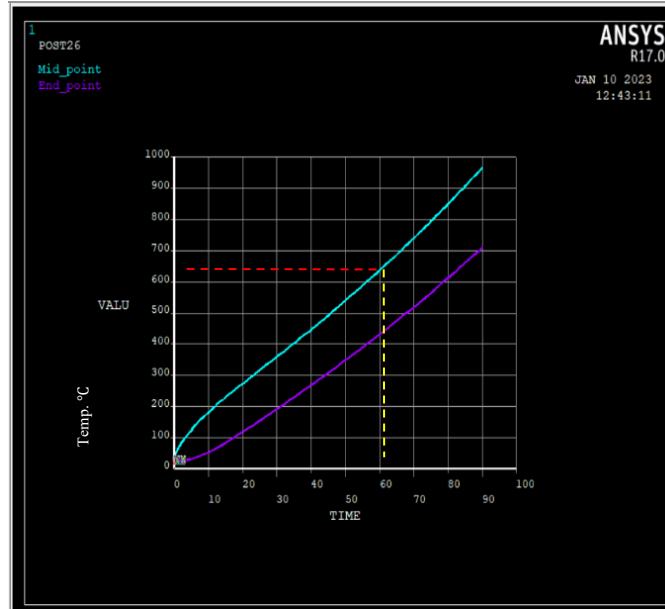


(b)

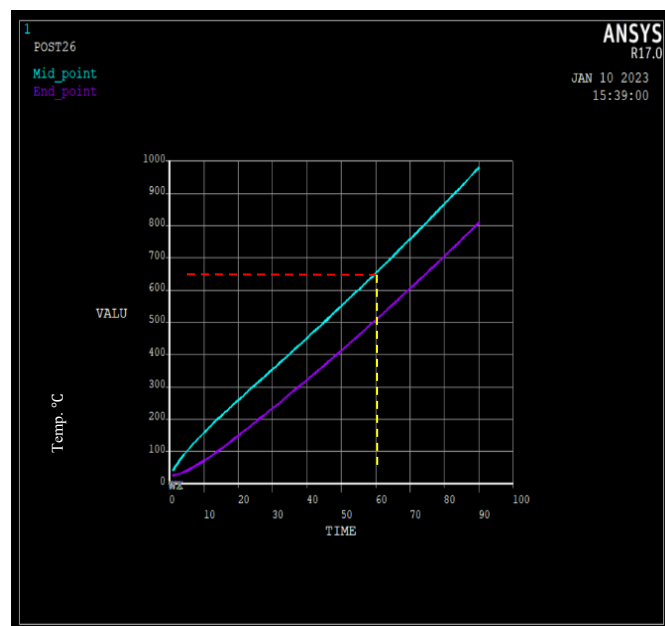
Fig. 4 The heat distribution in the workpiece (a) Coil A and (b) Coil B

The resistance of these parts must be added to the value of the ordinary series resistance of the coil due to its considerable effect of the resonance frequency of the tank circuit as shown in the following relation:

$$f_r = \frac{1}{2\pi} \sqrt{\frac{1}{LC} - \left(\frac{R_s}{L}\right)^2} \quad (11)$$



(a)



(b)

Fig. 5 Temperatures increase vs. time of two points on the workpiece, middle point and end point for both, (a) Coil A, (b) Coil B

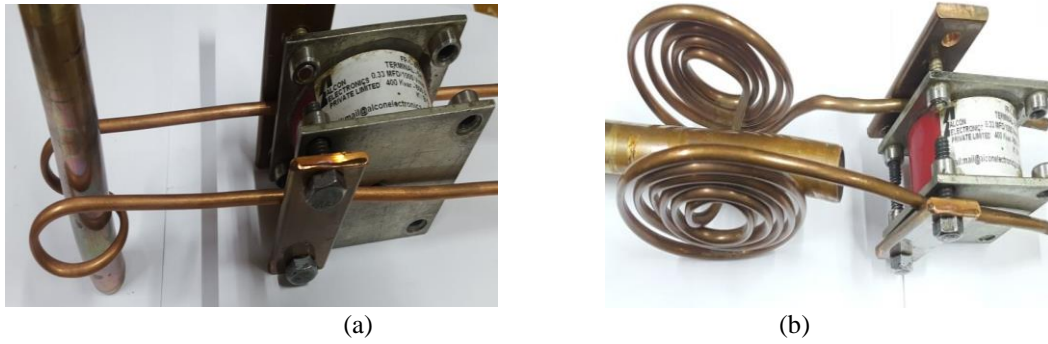


Fig. 6 Tank circuit of Coil A and B with the workpiece (a) Coil A (b) Coil B

R_s represents the equivalent resistance of the IC which is composed of three parts these are the ordinary resistance of the copper tube forming the coil body, the reflected resistance of the specimen, and that of the practical connection parts to form the tank circuit. This value is very essential to be considered in the analysis because its increase leads to reduce the resonance frequency. This relation is considered for a certain parallel tank circuit of self-inductance ($L = 1 \mu\text{H}$) for Coil A with resonance capacitance $C_o = 22 \mu\text{F}$, ($L = 3.7 \mu\text{H}$) for Coil B with resonance capacitance $C_o = 20 \mu\text{F}$.

IC's in IH furnaces are typically made of a hollow conductor that allows cooling water to circulate, and these hollow conductors are coated with thermal and electrical insulators. Because of this, a reasonable space between turns must exist [13], [25]. Hence, it differs in geometry from typical coils. In addition, the induced eddy currents in a conducting and non-magnetic specimen will be large. Figure 7 shows the equivalent circuit of the tank circuit [26].

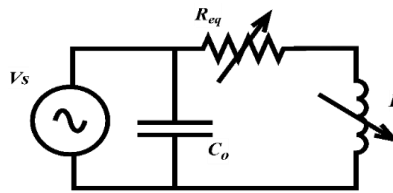


Fig. 7 Simple parallel resonant tank circuit

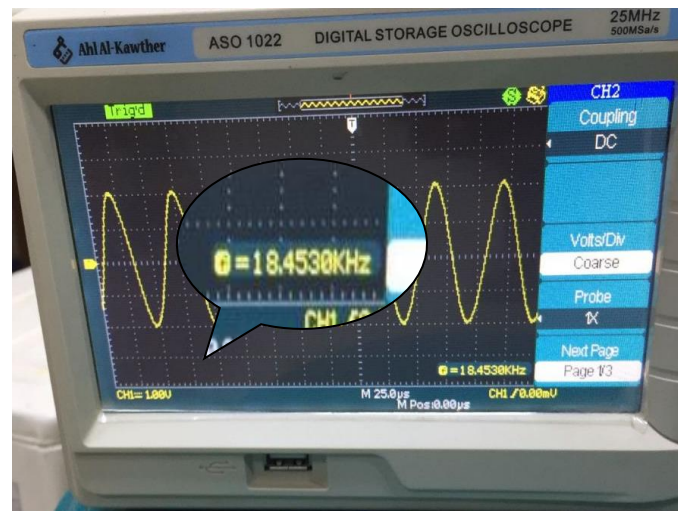


Fig. 8 Sinusoidal voltage waveform of $V_{tank_{max}} = 200 \text{ V}$ across the tank circuit.

Testing Coil B practically, the resonant voltage at the tank circuit of peak value of 200 V as shown in Figure 8. (Using an oscilloscope lead attenuated by a ratio of 1:100). The heated workpiece reaching temperature of 618 °C is shown in Figure 9. The calculated reactive power for induction coil equal to 46.386 kVAR. Table 2 illustrate the final comparison between the analytical and practical results, which improves the validity of the analytical algorithm.

$$f_r = 18.5 \text{ kHz}$$

$$X_{L_c} = 2\pi f_r L_c = 2\pi \times 18500 \times 3.7 \times 10^{-6} = 0.43 \ \Omega$$

$$V_{tank_{max}} = 200 \text{ V}, V_{tank_{rms}} = \frac{200}{\sqrt{2}} = 141.42 \text{ V}$$

$$I_{c_{rms}} = \frac{V_{tank_{rms}}}{X_{Lc}} = \frac{141.42}{0.43} = 328 \text{ A}, I_{c_{max}} = 328 \times \sqrt{2} = 465 \text{ A}$$

$$\text{kVar} = \frac{I_{c_{rms}} \times V_{tank_{rms}}}{1000} = \frac{328 \times 141.42}{1000} = 46.386 \text{ kVar}$$

Because of the shape of Coil (A) it cannot achieve the required brazing time with this power and frequency. Hence, several analytical iterations indicate that the coil could do this job by increasing the tank voltage up to 400 V_{max} and frequency up to 34 kHz.



Fig. 9 Practical test for Coil B

TABLE II. Comparison between analytical and practical results for Coil B

Parameters	Analytical	Practical	Unit
Frequency	18500	18500	Hz
Current	465	465	A
Time	56	52	s

VI. CONCLUSIONS

This work leads to many conclusions, these are:

- a- Each coil's design parameters are chosen after a lengthy procedure, as all parameters are dependent on current density, current frequency, geometry, time, and temperature. Extensive investigations were undertaken to achieve a suitable value for each of these characteristics for each coil. To keep the focus on the research goal, these attempts are not mentioned in the content of this paper.
- b- Because the practical resonance frequency is affected by the tank circuit's connection requirements, it differs from theoretical calculations and must be determined experimentally in a real tank circuit.
- c- Depending on the application, the induction coil geometry might be of various shapes. To establish the parameters of any geometrical shape, an Electromagnetic-Thermal coupled analysis must be performed. Coil A as shown in Figure 2 (a) is smaller in size than Coil B, so it could be used in cramped spaces where bigger coil like Coil B shown in Figure 2 (b) could not be used.
- d- Coil A generate heat in the workpiece in smaller area than Coil B, while Coil B generate heat in a larger area, so it could be used not only for joining the ends of two pipes, but also for fixing a crack in the workpiece by moving the coil along it.
- e- The simulation's results cannot be matched in practice. This is because the high frequency, high current circuit is extremely sensitive to the geometry of the connections. Furthermore, exact component values, such as tank capacitance, are not commercially available. As a result, the obtained results lead to a better understanding of the system's behavior.

REFERENCES

- [1] V. Rudnev, D. Loveless, and R. L. Cook, "Handbook of Induction Heating," Second Edition, Taylor & Francis Group, USA, 2017.
- [2] S. Zinn and L. Semiatin, "Elements of Induction Heating: Design, Control, and Applications," ASM International, 1988.
- [3] Y. V. Deshmukh, "Industrial Heating Principles, Techniques, Materials, Applications, and Design," Taylor & Francis Group, LLC, New York, USA, 2005.
- [4] V. Rudnev, D. Loveless and R. Cook, "Handbook of Induction Heating," Marcel Dekker Inc., New York, USA, 2003.
- [5] M. K. Panjwani, S. X. Yang, F. Xiao, K. H. Mangi, R. M. Larik, F. H. Mangi, M. Menghwar, J. Ansari, K. H. Ali, "Hybrid Concentrated Photovoltaic Thermal Technology for Domestic Water Heating," *Indonesian Journal of Electrical Engineering and Computer Science*, vol. 16, no. 3, pp. 1136–1143, 2019, doi: 10.11591/ijeecs.v16.i3.pp1136-1143.

- [6] Firas A. Rasheed and I. M. Abdulbaqi, "Design, Simulation and Implementation of a Self Tuned Single-Phase Inverter for Induction Furnaces Applications," MSc. Thesis, Collage of Engineering, University of Mustansiriyah, Iraq, 2022.
- [7] American Welding Society (AWS), "Brazing Handbook," Fifth Edition, Miami, USA, 1991.
- [8] D. Fleisch, "A Student's Guide to Maxwell's Equations," Cambridge University Press, 2008.
- [9] A. F. Salman, F. A. Rasheed & I. M. Abdulbaqi, "Design and Simulation of a Special Medium Power Induction Heating System for Oxygen Free Copper Production," *Journal of Engineering and Sustainable Development*, 2nd online Scientific conference for Graduate Engineering Students, 1-34-1-41, (2021). <https://doi.org/10.31272/jeasd.conf.2.1.5>.
- [10] Y. Lefevre, C. Henaux, and J. F. Llibre, "Magnetic Field Continuity Conditions in Finite-Element Analysis," *IEEE Transactions on Magnetics*, vol. 54, no. 3, pp. 7400304/1-7400304/4, 2018, doi: 10.1109/TMAG.2017.2762084.
- [11] I. J. Jebur and K. R. Hameed, "Evaluation and improvement of the main insulation structure of 33kV distribution transformer based on FEM," *Indonesian Journal of Electrical Engineering and Computer Science*, vol. 15, no. 1, pp. 36-47, 2019, doi: 10.11591/ijeecs.v15.i1.pp36-47.
- [12] M. H. Khazaal, I. M. Abdulbaqi, & R. H. Thejel, "Modeling, design and analysis of an induction heating coil for brazing process using FEM," *Al-Sadiq International Conference on Multidisciplinary in IT and Communication Techniques Science and Applications*, AIC-MITCSA 2016, 99-104, 2016. <https://doi.org/10.1109/AIC-MITCSA.2016.7759918>.
- [13] Dragomir and Nikolay, "Numerical Design of Complex Chape Coils," XVI-th International Conference on Electrical Machines, Drives and Power Systems ELMA 2019, 6-8 June 2019, Varna, Bulgaria, doi: 10.1109/ELMA.2019.8771642.
- [14] H. Kamil, F. Hamdan, F. Abbas & I. M. Abdulbaqi, "Design and Simulation of a Portable Copper Tubes Induction Brazing Tool for PV System Application," *Journal of Physics: Conference Series*, 1804 (1), 0-10, 2021. <https://doi.org/10.1088/1742-6596/1804/1/012094>.
- [15] Aziz Sh. Hamad, "A Novel Technique for A Portable Induction Welding Machine," MSc. Thesis, Collage of Engineering, University of Mustansiriyah, Iraq, 2021.
- [16] H. F. Sabeeh, I. M. Abdulbaqi, and S. M. Mahdi, "A 3D FEA Approach to Design an Induction Coil for Case Hardening of a Carbon Steel Gear," *3rd Scientific Conference of Electrical Engineering (SCEE)*, pp. 327-332, 2018, doi: 10.1109/SCEE.2018.8684208.
- [17] Richard E. Haimbaugh, "Theory of Heating by Induction," in *Practical Induction Heat Treating*, Second Edition, ASM International, USA, 2015.
- [18] Hamdan F. Sabeeh, Isam M. Abdulbaqi, Sahib M. Mahdi, "Design and Implementation of Induction Coil for Case Hardening of a Carbon Steel Gear," *Journal of Advanced Electromagnetics*, Vol. 9, No. 3, pp. 47-55, December 2020.
- [19] ANSYS Inc., "ANSYS Mechanical APDL Low-Frequency Electromagnetic Analysis Guide," Release 15.0, 2013.
- [20] A. Khati, A. Kansab, R. Taleb, and H. Khouidmi, "Current Predictive Controller For High Frequency Resonant Inverter In Induction Heating," *International Journal for Electrical Computer Engineering*, vol. 10, no. 1, pp. 255-264, 2020, doi: 10.11591/ijece.v10i1.pp255-264.
- [21] B. Djamel, H. Houassine, N. Kabache, and D. Moussaoui, "Electromagnetic Nonlinear Parametric Study of The Synrm Using FEM Method," *Indonesian Journal of Electrical Engineering and Computer Science*, vol. 24, no. 2, pp. 637-648, 2021, doi: 10.11591/ijeecs.v24.i2.pp637-648.
- [22] R. A. Higgins, "Metallurgical Principles of the Joining of Metals," in *Engineering Metallurgy*, Sixth Edition Arnold, New York, USA, 1999.
- [23] ANSYS Inc., "ANSYS Mechanical APDL Command Reference," Release 13.0, 2010.
- [24] ANSYS Inc., "Mechanical APDL Modeling and Meshing Guide," Release 13.0, 2010.
- [25] V. Geetha and V. Sivachidambaranathan, "An Overview Of Designing An Induction Heating System For Domestic Applications," *Internatonal Journal of Power Electronic and Drive Systems*, vol. 10, no. 1, p. 351, 2019, doi: 10.11591/ijpeds.v10.i1.pp351-356.
- [26] P. Herasymenko and V. Pavlovskiy, "Soft Start-Up Strategy of Pulse-Density-Modulated Series-Resonant Converter for Induction Heating Application," *Internatonal Journal of Power Electronic and Drive Systems*, vol. 12, no. 1, pp. 258-272, 2021, doi: 10.11591/ijpeds.v12.i1.pp258-272.